Energy & Environmental Science

COMMUNICATION

View Article Online
View Journal | View Issue

Voltage output of efficient perovskite solar cells with high open-circuit voltage and fill factor†

Cite this: *Energy Environ. Sci.*, 2014, 7, 2614

Received 8th March 2014
Accepted 16th May 2014

DOI: 10.1039/c4ee00762j

www.rsc.org/ees

Seungchan Ryu,‡[a] Jun Hong Noh,‡[a] Nam Joong Jeon,[a] Young Chan Kim,[a] Woon Seok Yang,[a] Jangwon Seo[a] and Sang Il Seok*[ab]

Besides the generated photocurrent as a key factor that impacts the efficiency of solar cells, the produced photovoltage and fill factor are also of critical importance. Therefore, understanding and optimization of the open-circuit voltage (V_{oc}) of perovskite solar cells, especially with an architecture consisting of mesoporous (mp)-TiO_2/perovskite/hole transporting materials (HTMs), are required to further improve the conversion efficiency. In this work, we study the effects of the energy level between CH_3NH_3(= MA)PbI_3 and $MAPbBr_3$ and a series of triarylamine polymer derivatives containing fluorene and indenofluorene, which have different highest occupied molecular orbital (HOMO) levels, in terms of the photovoltaic behaviour. The voltage output of the device is found to be dependent on the higher energy level of perovskite solar absorbers as well as the HOMO level of the HTMs. The combination of $MAPbBr_3$ and a deep-HOMO HTM leads to a high photovoltage of 1.40 V, with a fill factor of 79% and an energy conversion efficiency of up to 6.7%, which is the highest value reported to date for $MAPbBr_3$ perovskite solar cells.

Broader context

Increasing the efficiency and lowering the cost of photovoltaic devices are important targets of the current research. Recently, organolead trihalide perovskites as light harvesters have provided a breakthrough for achieving potentially low-cost and high efficiency solar cells. For further improvement of the performance, an understanding and optimization of the open-circuit voltage (V_{oc}) of the perovskite solar cells, especially with an architecture consisting of perovskite-infiltrated TiO_2 electrode/upper perovskite/hole transporting materials (HTMs), are very important. Although high V_{oc} in the perovskite solar cell can be achieved by matching and judiciously selecting the perovskite lead halide-based absorber and the HTMs, the origin of V_{oc} in the cell architecture is poorly understood. In this work, we have investigated the effect of lowering the highest occupied molecular orbital (HOMO) of the HTM using a series of triarylamine polymer derivatives. The results revealed that the voltage output of the device is found to be dependent on the higher energy level of perovskite solar absorbers as well as the HOMO level of the HTMs. We found that a deeper HOMO resulted in a significantly larger V_{oc}, which enabled us to fabricate high-efficiency solar cells with a V_{oc} of up to 1.40 V and a fill factor (FF) of 79% as well as a PCE of 6.7%.

Efficient and inexpensive energy harvesting by solar cells is a great challenge for the 21st century in the field of renewable energy. Most recently, inorganic–organic hybrid solar cells have been demonstrated to be amongst the most promising emerging photovoltaic devices with respect to the power conversion efficiency (PCE), use of liquid-free hole-conductors as charge carriers, abundant availability, and inexpensive fabrication.[1–8] Mesoscopic inorganic–organic hybrid heterojunction solar cells consisting of Sb_2S_3 or a combination of Sb_2S_3 and Sb_2Se_3 as light harvesters have shown a PCE of 3–7.5%.[1–4] Inorganic light harvesters in these cells have high potential to further improve the performance as compared to the conventional dyes, owing to benefits such as high extinction coefficients, large intrinsic dipole moments, and easily tuneable band-gaps.[9] A breakthrough in PCE for inorganic–organic hybrid solar cells has been achieved by the introduction of organolead trihalide perovskites as light harvesters.[5–8] Previously, these perovskites were used for light absorption in dye-sensitized solar cells with liquid electrolytes, which exhibit a low PCE.[10,11] However, the photovoltaic (PV) efficiency of the perovskite-based solar cells could be greatly improved by the use of a spiro-OMeTAD-based or polymeric solid hole-conductor.[5–8] The PCE was further improved by the sequential process of PbI_2 and CH_3NH_3I (methylammonium iodide: MAI) to deposit $CH_3NH_3PbI_3$ (=$MAPbI_3$) perovskites on a mesoporous (mp)-TiO_2 electrode,[12] and a planar thin layer of $MAPbI_{3-x}Cl_x$ was deposited by the vacuum thermal evaporation method without the mp-TiO_2 electrode.[13]

[a]*Division of Advanced Materials, Korea Research Institute of Chemical Technology, 141 Gajeong-Ro, Yuseong-Gu, Daejeon 305-600, Republic of Korea. E-mail: seoksi@krict.re.kr; seoksi@skku.edu*

[b]*Department of Energy Science, Sungkyunkwan University, 2066 Seoburo, Jangan-gu, Suwon 440-746, Republic of Korea*

† Electronic supplementary information (ESI) available: A description on the detailed experimental process and characterization. See DOI: 10.1039/c4ee00762j

‡ These two authors contributed equally to this work.

In addition, the perovskite was justifiably utilized as a donor in organic photovoltaic architectures because of its large diffusion length.[14,15] Thus, the unusual properties of the perovskites could be exploited for thin-film planar, meso-superstructured, or mesoporous architectures in perovskite-sensitized solar cells. However, we recently proposed that a bi-layer architecture consisting of the perovskite-infiltrated mp-TiO_2 and pure perovskite is crucial in fabricating efficient perovskite cells with coincident reverse and forward scans.[16]

Generally, high open-circuit voltage (V_{oc}) solar cells are important tools for driving electrochemical reactions or adopting new device architectures, such as the top-cell in tandem solar cell structures. Hodes and co-workers[17] demonstrated a high V_{oc} of 1.5 V from a solar cell based on the organic–inorganic lead bromide and 4,4′-bis(*N*-carbazolyl)-1,1′-biphenyl (CBP) hybrid structure, but the efficiency was low. J. Qiu *et al.*[18] described organolead halide perovskite cells, with $CH_3NH_3PbBr_3$ as the light harvester and poly[*N*-90-heptadecanyl-2,7-carbazole-*alt*-3,6-bis-(thiophen-5-yl)-2,5-dioctyl-2,5-dihydropyrrolo[3,4]pyrrole-1,4-dione] (PCBTDPP) as the hole transporting material (HTM), which showed a V_{oc} of 1.16 V and an efficiency of 3.04%, which is the highest observed for solid state $MAPbBr_3$ devices to date. Nevertheless, to the best of our knowledge, $MAPbBr_3$ perovskite solar cells that have PCEs exceeding 6% with V_{oc} approaching 1.4 V have not yet been reported. It is necessary to determine how and where the V_{oc} is established for understanding the PV performance and its optimization. In particular, the origin of V_{oc} in the bilayer cell architecture consisting of mp-TiO_2–perovskite/perovskite/HTM, which is significantly different from conventional dye-sensitized solar cells, is poorly understood. A high V_{oc} in the perovskite solar cell can be achieved by matching and judiciously selecting the perovskite lead halide-based absorber and the HTMs.

Here, we have investigated the effect of lowering the highest occupied molecular orbital (HOMO) of the HTM to enhance the V_{oc} of mesoscopic perovskite solar cells. We found that a deeper HOMO results in a significantly larger V_{oc}, which enabled us to fabricate high-efficiency solar cells with a V_{oc} of up to 1.40 V and a fill factor (FF) of 79% as well as a PCE of 6.7%, the highest values ever reported for $MAPbBr_3$perovskite solar cells.

Inorganic–organic hybrid solar cells were fabricated in the configuration mesoporous (mp)-TiO_2/perovskite/HTM/Au. Both the light absorber ($MAPbBr_3$ or $MAPbI_3$ perovskites) and the HTM were deposited onto mp-TiO_2 by spin coating. The homogeneous perovskite layer was deposited with full coverage on mp-TiO_2 (see Fig. S1†) The HTMs used in this work are triarylamine (TAA) polymer derivatives containing fluorene and indenofluorene, named P-TAA, PF8-TAA, and PIF8-TAA; the molecular structures of these are shown in Fig. 1a.[19] First, we measured the valence bands of $MAPbBr_3$ and $MAPbI_3$ perovskites, and the HOMO levels of HTMs, which are P-TAA, PF8-TAA, and PIF8-TAA, because the V_{oc} in solar cell devices can be derived from the quasi-Fermi levels of each material in the structure. Fig. 1b shows the photoelectron emission spectra of $MAPbI_3$, $MAPbBr_3$, PTAA, PF8-TAA, and PIF8-TAA obtained using a Riken Keiki AC-2 photoelectron spectrometer.

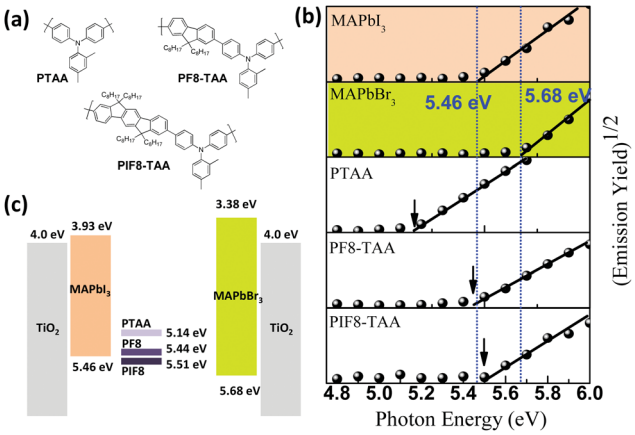

Fig. 1 (a) Molecular structure of HTMs (PTAA, PF8-TAA, and PIF8-TAA); (b) PESA spectra of perovskite films ($MAPbI_3$ and $MAPbBr_3$) and HTM films on a fused silica substrate; (c) energy band diagram for TiO_2, perovskite materials ($MAPbI_3$ and $MAPbBr_3$), and HTMs.

Photoelectron spectroscopy (PES) measurements were successfully performed to measure the occupied electronic states of an organic semiconductor and the valence band edges (VBEs) in solids.[20–22] The measured VBEs of $MAPbI_3$ and $MAPbBr_3$ were −5.46 eV, which is in accord with the reported values,[6] and −5.68 eV, respectively. The HOMO levels of P-TAA, PF8-TAA, and PIF8-TAA were measured to be −5.14 eV, −5.44 eV, and −5.51 eV which are in accord with a previous report.[19] The band alignment is represented in Fig. 1c, where the conduction band edge is calculated from the optical band gap of the perovskite materials. The excited state of the perovskite is higher than the TiO_2 conduction band, and the HOMO levels of PF8-TAA and PIF8-TAA are located near the valence band edges of $MAPbI_3$ and $MAPbBr_3$, respectively.

Fig. 2a shows the diffuse reflectance of $MAPbBr_3$ deposited on the mp-TiO_2/blocking layer (bl)-TiO_2/FTO substrate, which was measured using a UV-Vis spectrometer with an integrated sphere. The optical band gap of $MAPbBr_3$ is calculated to be 2.3 eV from the diffuse reflectance spectra. Fig. 2b shows the *J*–*V* characteristics of the FTO/bl-TiO_2/mp-TiO_2:$MAPbBr_3$/HTM-devices with different HTMs of PTAA, PF8-TAA, and PIF8-TAA measured under AM 1.5 illumination conditions. Table 1 summarizes the extracted short-circuit current density (J_{sc}), V_{oc}, and fill factor (FF). V_{oc} increased with the deeper HOMO of the HTMs, from 1.29 V of P-TAA to 1.36 V of PF8-TAA and 1.40 V of PIF8-TAA. This reveals that the HOMO level of the HTM influences V_{oc}. The origin of V_{oc} in perovskite solar cells is typically described by the difference between the lowest unoccupied molecular orbital (LUMO) level of the perovskite and the HOMO of the HTM, or by the potential difference between the quasi-Fermi level of the electron (E_{fn}) at the electron extracting layer/anode interface and the quasi-Fermi level of the hole (E_{fp}) at the hole extracting layer/cathode interface under illumination, assuming that recombination within the device can be ignored.[18,23] Therefore, the high V_{oc} of 1.40 V in the $MAPbBr_3$-PIF8(TAA)-device is ascribed to the deeper HOMO level near the VBE of $MAPbBr_3$. The determination of V_{oc} in the perovskite cell

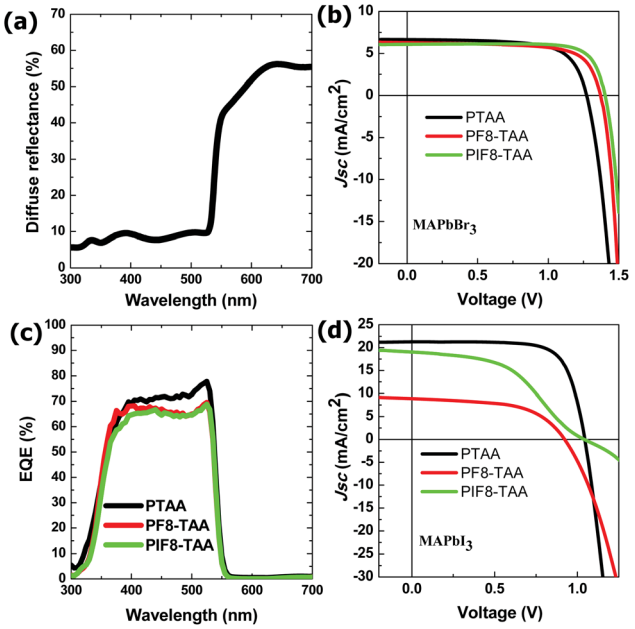

Fig. 2 (a) Diffused reflectance spectrum of FTO/bl-TiO_2/mp-TiO_2: $MAPbBr_3$/Au specimen; (b) *J–V* characteristics of FTO/bl-TiO_2/mp-TiO_2: $MAPbBr_3$/HTM/Au, where HTMs are PTAA, PF8-TAA, and PIF8-TAA; (c) EQE spectra; (d) *J–V* characteristics of FTO/bl-TiO_2/mp-TiO_2: $MAPbI_3$/HTM/Au with these three HTMs.

Table 1 Photovoltaic parameters for $MAPbI_3$ and $MAPbBr_3$ perovskite solar cells using PTAA, PF8-TAA, and PIF8-TAA as HTMs

Perovskite	HTMs	J_{sc} (mA cm^{-2})	V_{oc} (V)	FF	PCE (%)
$MAPbBr_3$	PTAA	6.6	1.29	0.70	5.9
	PF8-TAA	6.3	1.36	0.70	6.0
	PIF8-TAA	6.1	1.40	0.79	6.7
$MAPbI_3$	PTAA	21.3	1.04	0.73	16.2
	PF8-TAA	8.9	0.92	0.56	4.6
	PIF8-TAA	19.0	1.04	0.46	9.1

will be further discussed later. In Fig. 2b and Table 1, we also see that the increased V_{oc} accompanies a decrease in the photocurrent (J_{sc}), while the FF increases, in the sequence P-TAA, PF8-TAA, and PIF8-TAA. The external quantum efficiency (EQE) shown in Fig. 2c for devices using PIF-TAA and PIF8-TAA as HTMs is lower than that of P-TAA over the whole range of absorption wavelengths. The relatively low EQE and decreased J_{sc} with deeper HOMO levels of the HTMs might be attributed to the lowering of the driving force for charge injection, due to the small disruption in energy levels between the VBE of $MAPbBr_3$ and the HOMO of the HTM, as shown in Fig. 1b. In contrast, the remarkable FF of PIF8-TAA can be related to the charge carrier mobility (4×10^{-2} cm^2 V^{-1} s^{-1}) which is higher than that of PF8-TAA (2×10^{-2} cm^2 V^{-1} s^{-1}) and P-TAA (4×10^{-3} cm^2 V^{-1} s^{-1}).[19] The much larger driving force of P-TAA may counterbalance the low charge carrier mobility, resulting in the same FF as that of PF8-TAA. However, the FF might also be determined by other factors such as the charge injection rate and the recombination rate at the interface contact between perovskite and HTM.[24] Regardless of the reduced J_{sc}, the increase in V_{oc} and FF leads to an improved PCE of 6.7%. Consequently, the V_{oc}, FF, and PCE of 1.40 V, 79%, and 6.7%, respectively, are the highest among those reported for existing single-junction $MAPbBr_3$ perovskite solar cells. To ensure the reproducibility of the results, a histogram for the efficiencies of each cell is shown in Fig. S2.†

For the perovskite solar cell, especially for the architecture consisting of the mp-TiO_2–perovskite composite and pure perovskite layers, our previous results[7,8] suggested that the V_{oc} is not simply determined by the difference between the electron Fermi level at mp-TiO_2 and the hole Fermi level at the HTM. Under the current operation mechanism, the perovskite acts as an absorber as well as a charge (either electron or hole) carrier; hence, the voltage output is expected to be high since sensitization or donor–acceptor type devices significantly reduce the expected V_{oc} because of some charge transfer energy loss. Furthermore, perovskite has high capacitance and can accumulate charges on itself, because of which the quasi Fermi level is controlled upon illumination.[25]

To gain more insight into the V_{oc} of the perovskite cells with HTMs having a deeper HOMO, we additionally fabricated devices using $MAPbI_3$ with the same HTMs used in $MAPbBr_3$. Fig. 2d shows the *J–V* characteristics of $MAPbI_3$ perovskite solar cells using PTAA, PIF8-TAA, and PIF8-TAA as HTMs; the photovoltaic parameters are also summarized in Table 1. One can assume that E_{fn} is constant in FTO/bl-TiO_2/mp-TiO_2:perovskite/HTM-devices, although different HOMO levels of HTMs are used. It is noted that the HOMO levels of PTAA and PF8-TAA are −5.14 eV and −5.44 eV, respectively, which are higher than the VBE (−5.46 eV) of $MAPbI_3$ and therefore, hole transport from $MAPbI_3$ to the HTMs is favoured. However, PIF8-TAA has a lower HOMO level of −5.51 eV as compared to the VBE of $MAPbI_3$, which may result in a hole-injection barrier between $MAPbI_3$ and PIF8-TAA. The *J–V* curve of the FTO/bl-TiO_2/mp-TiO_2:$MAPbI_3$/PIF8-TAA-device shows the roll-over effect, in which the current is saturated at high forward bias, while the PTAA and PF8-devices show a typical *J–V* response. The roll-over effect has been explained by a back contact hole-injection barrier in CdTe, PbS, and organic solar cells.[26] Moreover, the driving force might be not enough for hole injection from $MAPbI_3$ to PF8-TAA because PF8-TAA has a similar HOMO level to the VBE in $MAPbI_3$, as shown in Fig. 1b. Therefore, it is difficult to discuss the effect of the HOMO level in HTMs on V_{oc} for $MAPbI_3$-devices, because of the insufficient driving force for charge injection and the abnormality in the *J–V* response. Nevertheless, the significantly high J_{sc} value of 19.0 mA cm^{-2} for the FTO/bl-TiO_2/mp-TiO_2: $MAPbI_3$/PIF8-TAA-device in spite of the unfavourable energetic alignment between $MAPbI_3$ and PIF8-TAA is an interesting result. Other effects except the energy level between perovskite and the HTM may affect charge transfer, because the perovskite material is known for its very low exciton binding energy or its ability to act as a free electron–hole carrier.[27]

J–V characteristics and photovoltaic parameters of $MAPbI_3$ and $MAPbBr_3$ fabricated with spiro-OMeTAD [(2,2′,7,7′-

tetrakis(*N*,*N*-di-*p*-methoxyphenylamine)-9,9′-spirobifluorene)] as low-molecular HTMs are given in Fig. S3 and Table S1.† We see that the use of spiro-MeOTAD, which has a higher HOMO level than that of PTAA, resulted in a decrease of the V_{oc} for both $MAPbI_3$ and $MAPbBr_3$. Therefore, our results further suggest that the energy level of the contact materials could have a strong impact on the deliverable energy of photoinduced charges. However, it is important to select energetically favourable contact materials with the HOMO well-aligned to the VBE of the perovskite to maximize the energy output.

Fig. 3a compares the *J*–*V* characteristics of $MAPbI_3$ and $MAPbBr_3$ perovskite solar cells using PTAA as the HTM. The cross-sectional image of a representative device is shown in the inset of Fig. 3a. Comparison of the V_{oc} value of FTO/bl-TiO_2/mp-TiO_2:$MAPbBr_3$/PTAA with that of FTO/bl-TiO_2/mp-TiO_2:$MAPbI_3$/PTAA shows that V_{oc} can be increased from 1.04 V to 1.29 V simply by changing the perovskite material from $MAPbI_3$ to $MAPbBr_3$ in the same sandwich structure between mp-TiO_2 and PTAA. This result reveals that the perovskite materials obviously contribute to E_{fn} and E_{fp} within the device. As shown in Fig. 1b, $MAPbBr_3$, with a wider band gap (2.3 eV) than $MAPbI_3$ (1.55 eV), has a lower VBE (5.68 eV) and a higher conduction band edge (CBE, 3.38 eV) as compared to $MAPbI_3$. Therefore, when E_{fn} and E_{fp} are built-up within the device under light illumination, $MAPbBr_3$ might lead to a larger difference between E_{fn} and E_{fp} as compared to $MAPbI_3$, in spite of using the same electron (TiO_2) and hole extracting layers (PTAA), thus resulting in a higher V_{oc}. This is not expected in sensitized solar cells, because the FTO/bl-TiO_2/mp-TiO_2:$MAPbBr_3$/PTAA/Au device shows a higher V_{oc} of 1.29 V than the potential difference (1.16 eV) between the CBM (−4.0 eV) of TiO_2 and the HOMO level (−5.16 eV) of PTAA. Consequently, as depicted in Fig. 3b, the CBE level of the $MAPbBr_3$ can manipulate the voltage output of the mp-TiO_2–perovskite/perovskite/HTM bilayer junction cell. Based on this reasoning, a remarkably high voltage (1.40 V) device has been realized by judicious selection of the perovskite and HTM.

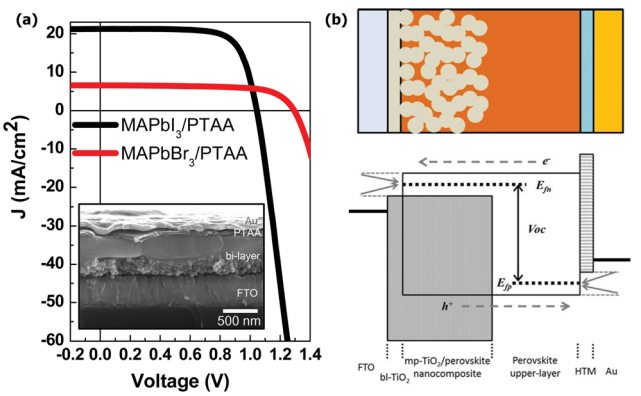

Fig. 3 (a) *J*–*V* characteristics of $MAPbI_3$-PTAA, and $MAPbBr_3$-PTAA devices. The inset shows a cross-sectional SEM image of the bi-layer architecture device (FTO/bl-TiO_2/mp-TiO_2:$MAPbBr_3$/PTAA/Au). (b) Schematic of the bi-layered device architecture and its energy band diagram. E_{fn} and E_{fp} are the electron and hole quasi-Fermi levels, which are determined by the interaction between TiO_2 and the perovskite and between the perovskite and the HTM, respectively.

This also means that the energy gap with charge separation significantly dominates the voltage output.

Summary

In summary, we have fabricated mp-TiO_2/$MAPbI_3$ and $MAPbI_3$ perovskite as the light harvester, and P-TAA, PF8-TAA, PIF-TAA as HTMs. The V_{oc} of $MAPbBr_3$ perovskite cells increased from 1.29 V of P-TAA to 1.36 V of PF8-TAA and 1.40 V of PIF8-TAA with a deeper HOMO level. In addition, the V_{oc} decreased from 1.29 V to 1.04 V by using $MAPbI_3$ in place of $MAPbBr_3$ with the same configuration and HTM (PTAA). This result reveals that both the perovskite materials and the HOMO level of the HTM determine the high voltage output in our devices. The $MAPbBr_3$-based perovskite device displayed a remarkably higher V_{oc} of 1.40 V, with an FF of 79%, due to the deep HOMO level and superior hole mobility, as well as a high PCE of 6.7%, when PIF8-TAA was used as the HTM. The present study demonstrates the main roles of the HTMs and perovskite light harvester in determining the V_{oc} and provides a suitable strategy for the design and development of perovskite-based solar cells showing a high V_{oc}, FF, and significantly improved PCE.

Acknowledgements

This work was supported by the Global Research Laboratory (GRL) Program, the Global Frontier R&D Program on Center for Multiscale Energy System funded by the National Research Foundation in Korea, and by a grant from the KRICT 2020 Program for Future Technology of the Korea Research Institute of Chemical Technology (KRICT), Republic of Korea.

Notes and references

1 J. A. Chang, S. H. Im, Y. H. Lee, H.-J. Kim, C.-S. Lim, J. H. Heo and S. I. Seok, *Nano Lett.*, 2012, **12**, 1863–1867.
2 Y. C. Choi, T. N. Mandal, W. S. Yang, Y. H. Lee, S. H. Im, J. H. Noh and S. I. Seok, *Angew. Chem., Int. Ed.*, 2014, **53**, 1329–1333.
3 Y. C. Choi, Y. H. Lee, S. H. Im, J. H. Noh, T. N. Mandal, W. S. Yang and S. I. Seok, *Adv. Energy Mater.*, DOI: 10.1002/aenm.201301680.
4 Y. C. Choi, D. U. Lee, J. H. Noh, E. K. Kim and S. I. Seok, *Adv. Funct. Mater.*, DOI: 10.1002/adfm.201304238.
5 M. M. Lee, J. Teuscher, T. Miyasaka, T. N. Murakami and H. J. Snaith, *Science*, 2012, **338**, 643–647.
6 H.-S. Kim, C.-R. Lee, J.-H. Im, K.-B. Lee, T. Moehl, A. Marchioro, S.-J. Moon, R. Humphry-Baker, J.-H. Yum, J. E. Moser, M. Grätzel and N.-G. Park, *Sci. Rep.*, 2012, **2**(591), 1–7.
7 J. H. Heo, S. H. Im, J. H. Noh, T. N. Mandal, C.-S. Lim, J. A. Chang, Y. H. Lee, H. Kim, A. Sarkar, M. K. Nazeeruddin, M. Grätzel and S. I. Seok, *Nat. Photonics*, 2013, **7**, 486–491.
8 J. H. Noh, S. H. Im, J. H. Heo, T. N. Mandal and S. I. Seok, *Nano Lett.*, 2013, **13**, 1764–1769.
9 A. J. Nozik, *Chem. Phys. Lett.*, 2008, **457**, 3–11.

10 A. Kojima, K. Teshima, Y. Shirai and T. Miyasaka, *J. Am. Chem. Soc.*, 2009, **131**, 6050–6051.
11 J.-H. Im, C.-R. Lee, J.-W. Lee, S.-W. Park and N.-G. Park, *Nanoscale*, 2011, **3**, 4088–4093.
12 J. Burschka, N. Pellet, S.-J. Moon, R. Humphry-Baker, P. Gao, M. K. Nazeeruddin and M. Grätzel, *Nature*, 2013, **499**, 316–319.
13 M. Liu, M. B. Johnston and H. J. Snaith, *Nature*, 2013, **501**, 395–398.
14 S. D. Stranks, G. E. Eperon, G. Grancini, C. Menelaou, M. J. P. Alcocer, T. Leijtens, L. M. Herz, A. Petrozza and H. J. Snaith, *Science*, 2013, **342**, 341–344.
15 G. Xing, N. Mathews, S. Sun, S. S. Lim, Y. M. Lam, M. Grätzel, S. Mhaisalkar and T. C. Sum, *Science*, 2013, **342**, 344–347.
16 N. J. Jeon, J. H. Noh, Y. C. Kim, W. S. Yang, S. Ryu and S. I. Seok, *Nat. Materials* (in press).
17 E. Edri, S. Kirmayer, M. Kulbak, G. Hodes and D. Cahen, *J. Phys. Chem. Lett.*, 2014, **5**, 429–433.
18 B. Cai, Y. Xing, Z. Yang, W.-H. Zhang and J. Qiu, *Energy Environ. Sci.*, 2013, **6**, 1480–1485.
19 W. Zhang, J. Smith, R. Hamilton, M. Heeney, J. Kirkpatrick, K. Song, S. E. Watkins, T. Anthopoulos and I. McCulloch, *J. Am. Chem. Soc.*, 2009, **131**, 10814–10815.
20 H. Nishi, T. Nagano, S. Kuwabata and T. Torimoto, *Phys. Chem. Chem. Phys.*, 2014, **16**, 672–675.
21 B. I. MacDonald, A. Martucci, S. Rubanov, S. E. Watkins, P. Mulvaney and J. J. Jasieniak, *ACS Nano*, 2012, **6**, 5995–6004.
22 J. Hwang, E.-G. Kim, J. Liu, J.-L. Brédas, A. Duggal and A. Kahn, *J. Phys. Chem. C*, 2007, **111**, 1378–1384.
23 B. A. Gregg and M. C. Hanna, *J. Appl. Phys.*, 2003, **93**, 3605–3614.
24 E. J. Juarez-Perez, M. Wuβler, F. Fabregat-Santiago, K. Lakus-Wollny, E. Mankel, T. Mayer, W. Jaegermann and I. Mora-Sero, *J. Phys. Chem. Lett.*, 2014, **5**, 680–685.
25 H.-S. Kim, I. Mora-Sero, V. Gonzalez-Pedro, F. Fabregat-Santiago, E. J. Juarez-Perez, N.-G. Park and J. Bisquert, *Nat. Commun.*, 2013, **4**, 2242.
26 J. Gao, J. M. Luther, O. E. Semonin, R. J. Ellingson, A. J. Nojik and M. C. Beard, *Nano Lett.*, 2011, **11**, 1002–1008.
27 P. Docampo, J. M. Ball, M. Darwich, G. E. Eperon and H. J. Snaith, *Nat. Commun.*, 2013, **4**, 2761.

